Nano Research 2018, 11(4): 1757–1767
https://doi.org/10.1007/s12274-017-1704-2
Research Article
ISSN 1998-0124
CN 11-5974/O4

Dynamics and self-assembly of bio-functionalized gold nanoparticles in solution: Reactive molecular dynamics simulations

Susanna Monti[1,2] (✉), Giovanni Barcaro[3], Luca Sementa[3], Vincenzo Carravetta[3], and Hans Ågren[2,4]

[1] *CNR-ICCOM, Institute of Chemistry of Organometallic Compounds, Pisa 56124, Italy*
[2] *KTH Royal Institute of Technology, School of Biotechnology, Division of Theoretical Chemistry and Biology, Stockholm S-10691, Sweden*
[3] *CNR-IPCF, Institute of Chemical and Physical Processes, Pisa 56124, Italy*
[4] *Institute of Nanotechnology, Spectroscopy and Quantum Chemistry, Siberian Federal University, Svobodny pr. 79, 660041 Krasnoyarsk, Russia*

Received: 12 April 2017
Revised: 6 June 2017
Accepted: 8 June 2017

KEYWORDS
nanoparticle,
ReaxFF,
functionalization,
cross-linking,
biocompatibility

ABSTRACT

The self-assembling properties, stability, and dynamics of hybrid nanocarriers (gold nanoparticles (AuNPs) functionalized with cysteine-based peptides) in solution are studied through a series of classical molecular dynamics simulations based on a recently parametrized reactive force field. The results reveal, at the atomic level, all the details regarding the peptide adsorption mechanisms, nanoparticle stabilization, aggregation, and sintering. The data confirm and explain the experimental findings and disclose aspects that cannot be scrutinized by experiments. The biomolecules are both chemisorbed and physisorbed; self-interactions of the adsorbates and formation of stable networks of interconnected molecules on the AuNP surfaces limit substrate reconstructions, protect the AuNPs from the action of the solvent, and prevent direct interactions of the gold surfaces. The possibility of agglomeration of the functionalized nanoparticles, compared with the sintering of the bare supports in a water solution, is demonstrated through relatively long simulations and fast steered dynamics. The analysis of the trajectories reveals that the AuNPs were well stabilized by the peptides. This prevented particle sintering and kept the particles far apart; however, part of their chains could form interconnections (crosslinks) between neighboring gold vehicles. The excellent agreement of these results with the literature confirm the reliability of the method and its potential application to the modeling of more complex materials relevant to the biomedical sector.

1 Introduction

The present investigations descend from a series of progressive studies of cysteine on gold in solution [1–3], where the focus was on the possibility to realistically reproduce cleavage of the SH bond and chemisorption

Address correspondence to sapeptides@gmail.com

of the molecule through the formation of a covalent S–Au connection using an *ad-hoc* optimized reactive force field (ReaxFF). The mechanism was studied on different types of gold supports, such as periodic slabs with low-index faces and multi-faceted truncated octahedron nanoparticles (gold nanoparticles (AuNPs)). In all cases, the simulations were very effective and capable of providing a possible explanation for the formation of stable cysteine adsorbates by identifying preferential locations for physisorption and chemisorption. The deprotonation mechanism was characterized in terms of the time and energy barriers by disclosing substrate reconstruction and gold atom capture. The permanence of the adsorbed monolayer on the surfaces was reinforced by the dense network of hydrogen bonds that interconnected a significant portion of the molecules and several adatoms (surface reconstructions), which emerged from the interface and became part of the cysteine protective layer. Water was confined to the outer regions; only a few units were entrapped in the molecular network and remained close to the metal supports. Subsequently, the simulations were extended to the adsorption of cysteine dimers [3]. The results confirm the reliability of the method by unveiling the behavior of the dimers both in solution and at the gold-water interface, where they had the propensity to form staple motifs.

In sum, all the computational outcomes satisfactorily agree with the state-of-the-art theoretical and experimental findings [4–24], suggesting that the developed methodology could be confidently applied to investigate more complex and challenging scenarios. Among these, hybrid nanocarriers that control the release of their cargo by means of peptide-decorated AuNPs as end-capping agents [25] represent a very interesting extension. Indeed, peptides with several polar functional groups and thiol moieties are used as multi-dentate agents to enhance the colloidal stability of AuNPs and to prepare them for potential biological applications [26–36].

To improve the design of these devices for a more effective and concerted performance, the structural and dynamical properties of the various hybrid components require in-depth characterization, possibly at the atomic/molecular level. Such a description can be obtained through representative theoretical chemistry frameworks.

Such frameworks have been demonstrated recently in a series of investigations by T. R. Walsh and co-workers [21–24, 26, 27] on peptides and gold. For example, in one of these studies [26], the authors theoretically and experimentally examined specific peptide sequences, their mutations, and their binding on Au interfaces by considering both the thermodynamics and kinetics. They successfully predicted the adsorbed structures, the anchoring points of the peptides on the supports, the correlation between the stability of the AuNPs, and the structural disorder of the peptide chains, using classical advanced molecular dynamics (MD) simulations. Even though the theoretical methodology was unable to explore the reactivity of the various species, it was efficient and well designed to reproduce/explain/predict the experimental data.

The present work refines the classical view by giving an idea of the complex reactive scenario inside a solution of AuNPs that are partially decorated with peptides.

2 Models and methodology

A simplified computational model adequate for depicting the portion of the nanocarrier containing gold–biomolecule complexes was defined by considering the relatively short linear chain AGCGGCG (terminated with an acetyl group and an N-methyl moiety) as the ligand and one of the truncated octahedral AuNP structures (average size of approximately 35 Å) used in an earlier work [37] as the support. Both the peptide and the substrate were selected based on experimental findings. Indeed, peptides containing the GC motifs exhibited good stabilizing capping properties [32], they strongly and specifically bound to gold in aqueous solution through a multidentate connection, and could be engaged in multiple interactions with different AuNPs, eventually leading to particle aggregation by crosslinking [33, 34]. Small (20–40 Å) and large (100–200 Å) AuNPs could be proficiently decorated with the aforementioned sequence [34]; however, for large nanoparticles, the binding configurations and coverage of the deposited layers could hardly be analyzed because of the very small concentration of adsorbates in relation to the gold material.

This last experimental finding biased our choice toward the gold cluster mentioned above. Even though this was a relatively small nanoparticle, it was large enough to accommodate a representative number of peptides on its surface; thus, it could be effectively used to achieve our aims: 1) understanding peptide adsorption on nearly spherical supports and 2) disclosing self-aggregation of the biofunctionalized units.

To reduce the computational cost, we skipped the simulation of the extremely long adsorption process of the peptides dispersed in solution and started the simulations with elongated peptide configurations in their best Au-binding arrangement (i.e., already in contact with the AuNPs surfaces (partial coverage)). We were interested in characterizing the behavior of the peptides on the surface of the AuNPs in solution, and not the approaching path of the peptides toward the nanoparticles.

Thus, we preferred to start from a stable conformation of the chain with the sulfur atoms positioned near the surface instead of sampling all possible arrangements of the peptides on the AuNP surface, which is impossible from a computational point of view. In principle, the chosen orientation should favor the release of the sulfur hydrogen and the formation of a covalent bond with the surface. Moreover, partial coverage is useful to check the perturbing effect of water on peptides and nanoparticle structures.

The computational model designed for these studies consists of two AuNPs (1,505 atoms each), sufficient peptides to cover the nanoparticle surface (42 peptide chains made of 72 atoms each—neutral cysteines), and approximately 20,000 water molecules. All these components were inserted into a simulation box of approximately 74 Å × 88 Å × 98 Å in the x, y, and z directions, respectively (Fig. 1). The total model consisted of approximately 60,000 atoms.

Before starting the simulations, preliminary studies were performed to recover the peptide chain conformational ensemble in water at T = 300 K using both the classical force field (ff12SB) [38] available in the AMBER12 package [39] and ReaxFF.

Briefly, a peptide structure was optimized using density functional theory with the B3LYP functional and the 6-31G(d) basis set and inserted in a simulation box filled with TIP3P water molecules. Equilibration in the constant-temperature, constant-pressure ensemble (NPT ensemble; T = 300 K, P = 1 atm) was performed for approximately 1 ns, whereas the subsequent production, or sampling stage, was extended to approximately 50 ns.

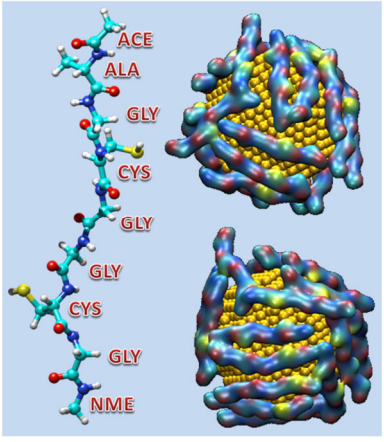

Figure 1 Peptide sequence adsorbed on the AuNPs in a water solution. Functionalized AuNPs inserted in a box of water (starting configuration; water was removed for clarity).

The sampled geometries were analyzed and selected by paying attention to the secondary structure, the mutual arrangement of the peptide sulfur atoms (which are important for binding to the substrate), and the orientation of the side chains (see Fig. S1 in the Electronic Supplementary Material (ESM)). Examination of the Ramachandran plot, which identifies the different areas of secondary structure, indicated that both beta-sheet and helical angles were densely populated, suggesting that this type of peptide is very mobile and flexible in solution. The most probable angle adopted by the cysteine side chain was approximately 60°, while the distance between the two sulfur atoms was within the interval of 7–15 Å with a maximum population at approximately 12 Å.

The ability of ReaxFF to correctly reproduce/evaluate the structures of the peptide was verified using a sample with different conformations that was randomly extracted from the classical trajectory, as done in a previous work [40]. The results were in line with the original parametrization, the structures were satisfactorily reproduced, and the data confirmed that the reactive representation could be used confidently to describe these peptide sequences.

When the peptide chains are adsorbed on the supports, their conformations are influenced by the substrates, neighboring peptide, and solvent molecules. Consequently, they could adopt constrained arrangements, which are favorable in those specific environments (i.e., well-balanced configurations in relation to the surrounding species).

To test the stability and dynamics of an optimal adsorbed peptide monolayer, we took advantage of the flexibility of the peptide and prepared partially covered AuNPs by selecting biomolecular conformations with trans sulfur atoms.

The SH groups were oriented toward the Au layer to start the simulations from a presumably favorable binding approach. The extended chains were placed on top of each AuNP in such a way that they could occupy all the regions of the surface, covering approximately 64% of the total area. Such a configuration enabled us to evaluate the effects of the water molecules located in regions not occupied by the peptides on the AuNPs and peptides. The two decorated AuNPs were initially located at an interparticle distance of approximately 25 Å (surface-to-surface) and well surrounded by water molecules. We would like to highlight that the AuNPs can also interact through periodic images with this specific choice of simulation box (as shown in Fig. S5 in the ESM). This further interaction influences the dimerization process and the response of the interparticle distance during the steering experiment.

MD simulations, based on the reactive force field parametrized in our earlier work [1] were carried out in the NPT ensemble at $T = 300$ K and ambient pressure, applying periodic boundary conditions in all directions. Temperature and pressure were controlled through the Berendsen's thermostat and barostat [41] with a relaxation constant of 0.1 ps. The time step was set at 0.25 fs during equilibration and at 0.50 fs throughout the production [40].

To reach a proper density, the initial equilibration was prolonged over a 3-ns period, whereas the subsequent sampling was performed for approximately 8 ns. The analysis presented in this report is focused on the last 800 ps of the production, and only the first configuration of this phase (i.e., the final structure of equilibration) is considered for comparison.

The ReaxFF version incorporated into the LAMMPs [42] program was used for all the simulations (named herein ReaxFF–MDs). The computational resources were provided by the CINECA consortium (Grant ISCRA 2016 SINGOLD).

Steered MD simulations in the NVT ensemble were also performed to test the behavior of functionalized and bare AuNPs in solution when the gold surfaces are at interacting distances. After pulling the two AuNPs at a surface–surface separation of approximately 7 Å, the pulling force was removed and the systems were simulated without constraints for approximately 400 ps.

3 Results and discussion

Major readjustments of all the peptide chains are observed during equilibration. These include changes in the conformations from extended to different degrees of bent structures, moderate migration of the molecules to other regions of the interface for improving self-interactions, and stretching portions of the chains toward the surrounding water molecules. Even though the initial arrangement should have favored the release of sulfur hydrogens and the formation of covalent bonds with the metal substrate, not all the peptides modify their protonation state, and some of them even detach from the supports. However, this relocation is confined to the second layer. There, the migrated peptides are attached to the molecules directly adsorbed on the surface. This replacement can be ascribed to the interactions between neighboring species, action of the surrounding water molecules, and surface reconstructions (adatoms) that are caused by the water and peptide action. Additionally, the peptides located on the areas of the AuNPs facing each other begin to self-interact and to induce rotation and translation of the whole particles to a closer distance within this time span. After equilibration, the final major species (in terms of cysteine protonation) are defined, and no relevant variations are observed during the subsequent simulation time. Both physisorbed and chemisorbed peptide chains are present on the interfaces.

As in a previous study [2], the stability and reorganization of the gold nanoclusters during the last 800 ps of the production phase were checked

by analyzing the radius of gyration (R_{gyr}) and the Au–Au radial distribution functions (Fig. S2 in the ESM), whereas the relocation of one of the AuNPs in relation to the other is described by examining both the motion of their centers of mass (cm) and the trend of the minimum distance between the two metal interfaces (Fig. 2).

The distributions of R_{gyr} and the radial arrangement of the atoms of both AuNPs, shown in Fig. S2 in the ESM, suggest that the initial crystallinity of the particles is preserved and no major changes of their bulk structures occur during their dynamics in solution in the presence of the adsorbate. Instead, a few superficial atoms, which are affected by the interaction with the surrounding species, escape from the surface and migrate to the outer layers of the supports.

Examination of the reconstruction reveals that the diffused atoms, which account for approximately 2% of the atoms, remain close to the particle surfaces (entrapped in the peptide network or captured by single peptide chains). Most of these adatoms are located near the boundaries of the most stable low-index patches, namely the (111) and (100) faces, and only a few (0.07%) are found at longer separations (approximately 12 Å, at most—refer to the inset in Fig. S2 in the ESM) and transform into incorporated coordinated metal atoms but are peripheral to the peptides molecules.

The motion of the biofunctionalized AuNPs in aqueous solution was characterized by a relatively fast translation and slower moderate rotations, which are both driven by the interactions between the biomolecules. The most striking displacement is observed just after equilibration (Fig. 2(a))—the initial distance of the particles (calculated in the first configuration before equilibration) is markedly reduced by approximately 4 Å in just 3 ns. Then, in the subsequent production phase, this separation decreases further, reaching a minimum of about 12 Å (starting point in the minimum distance plot of Fig. 2). However, within the last 800 ps of the production, the minimum distance remains in the range of 10.5–13.5 Å, confirming the propensity of the biofunctionalized nanoparticles to agglomerate through the mediating action of the peptides (crosslinking). The marked oscillations of the minimum distance in this range are essentially due

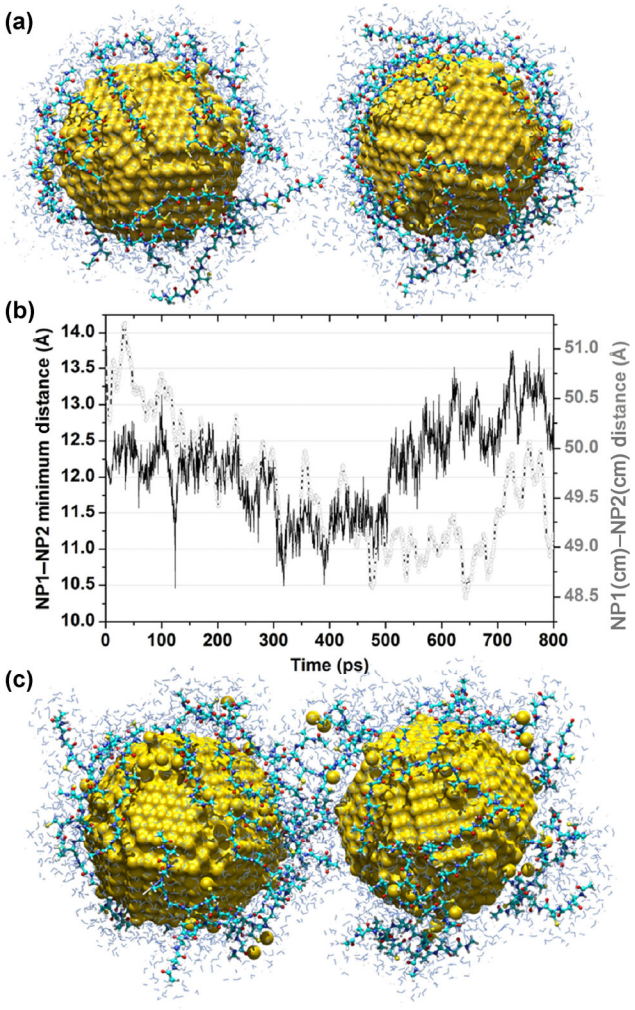

Figure 2 (a) Final configuration obtained after 3 ns of equilibration. (c) Final configuration obtained at the end of the production run (8 ns after equilibration). The peptide chains are shown as ball-and-stick models (red = O, cyan = C, blue = N, white = H, and yellow = S). Only the water molecules within 5 Å of the two AuNP/peptide complexes are displayed (blue lines). (b) AuNP(surface)–AuNP(surface) minimum distance and AuNP(cm)–AuNP(cm) distance vs. simulation time during the last 800 ps of the production stage.

to the relative rotations induced by the interactions of the adsorbates deposited on different particles. Indeed, in the final configuration (Fig. 2(c)) the interparticle region is densely occupied by the peptide chains that extend toward the opposite surface.

The final distribution of the species around the AuNPs is quite varied and far from the initial population where all the cysteine side chains are protonated (SH neutral forms). This is because 48% of the thiol groups maintain their hydrogens, whereas

the other 52% release them to the solvent and form a stable covalent interaction with gold. The variety of forms could be also defined based on the binding mode of the peptides: Only 29% are chemisorbed through both cysteine residues, whereas 52% use just one of them for binding. The rest of the molecules (19%) are neutral and are located farther from the interface but still in contact with the directly adsorbed species. This is apparent in Fig. 3, where the protonation state, connection to gold, and solvation of each sulfur atom are represented in terms of their minimum distances. The red and black lines at 1.6 and 2.6 Å, respectively, define the cutoff distances used to identify the S–H and S–Au bonds. All the S atoms are in contact with water (oxygen within 3.5 Å, blue triangles).

This was confirmed by examining various atom–atom radial distribution functions (Fig. S3 in the ESM). The

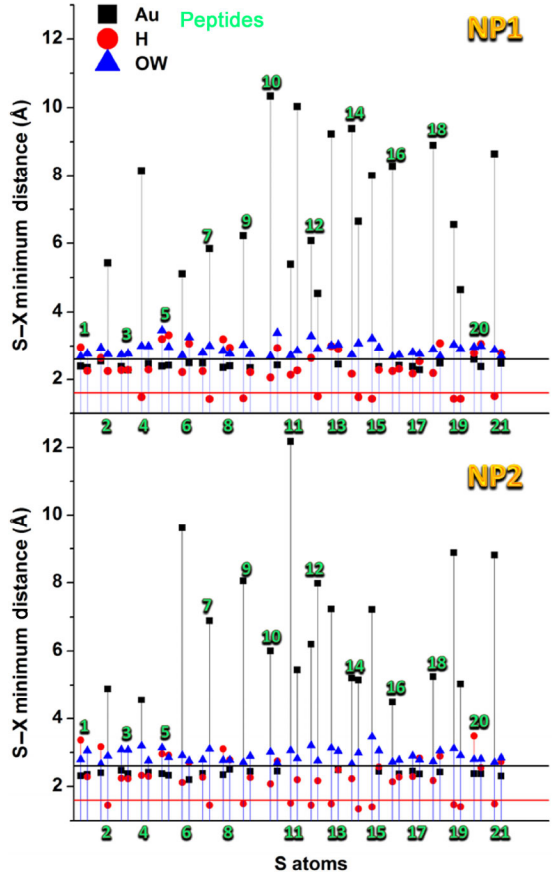

Figure 3 S–Au, S–H, and S–OW minimum distances of all the peptides distributed on the two AuNPs (NP1, NP2). Final configuration. Some of the Au–S minimum distances involve Au atoms that have detached from the surface and have migrated to the peptide shell.

S–X radial distribution function (RDF) plots clearly show that S is in contact with gold and surrounded by water oxygens, but it is also evident that carbonyl oxygen and nitrogen atoms are other possible binders.

Indeed, in agreement with the data displayed in Fig. 3, the first S–Au peaks are sharp and centered at approximately 2.3 Å, whereas those of water (S–water oxygen (OW)) are broader, lower, and located at a longer distance (approximately 2.8 Å). The carbonyl oxygen–Au RDFs have distinct tall peaks at approximately 2.5 Å, whereas nitrogen with its broad distributions seemed less inclined to remain adsorbed. Even if all the sharp peaks indicate stable adsorption of both S and O atoms of the peptide, the presence of a flat zero region between the first and the second peaks in the S–Au RDF plots provides a distinction, suggesting that the S–Au coordination is stronger than the O–Au bond. Indeed, when S is adsorbed in such a way, it remains almost immobile in the same location for the rest of the simulation time. The lack of the zero region in the RDF curves of O–Au suggests, instead, a higher mobility of these atoms on the metal support. This is probably ascribable to the perturbing action of the neighboring groups of the chain that are also involved in interactions with the substrate. Furthermore, in line with previous findings, S is preferentially found on bridge and hollow sites. Several peptide arrangements and adsorption configurations are shown in Fig. 4.

Other effective descriptors used to classify the structure of the peptides and their relative orientations are the interchain hydrogen bonds and the head-to-tail distances. This latter is useful for estimating the degree of chain folding (Fig. S4 in the ESM), whereas the former is practical for identifying the degree of association of the molecules. All the initially extended conformations (average length of approximately 27 Å) all suffer from major rearrangements that are driven by the tendency to balance adsorption, self-interaction, and solvation. During the production dynamics, they adopt more folded geometries with head-to-tail distances distributed in the range 7–24 Å and become closer to each other, exposing large areas of the supports to the action of the solvent (Fig. 4 and Fig. S5 in the ESM). Indeed, the coverage (which was initially approximately 50%) is reduced to 38% at the end of

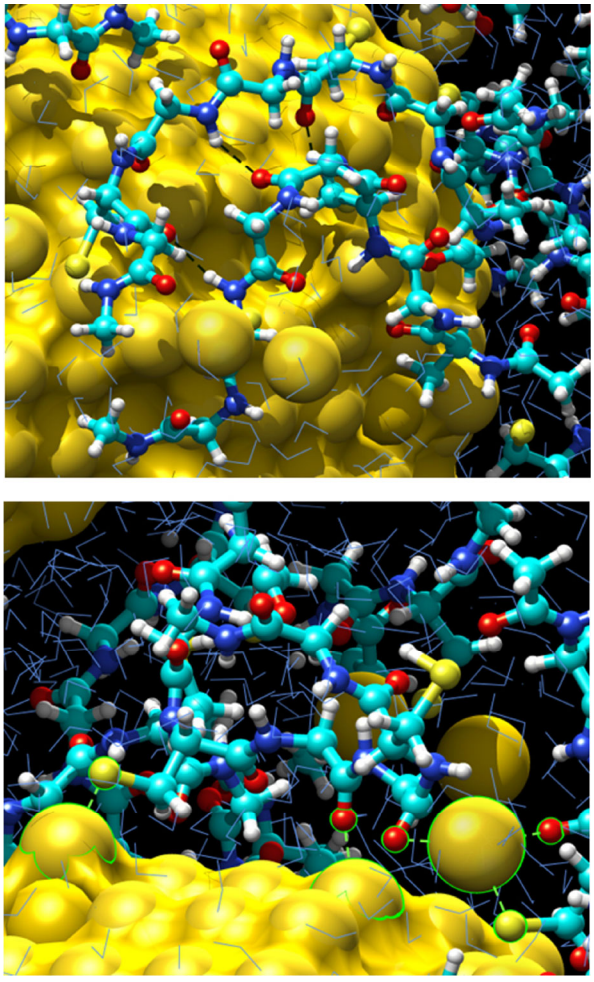

Figure 4 Different regions of the AuNPs functionalized with peptides. Sulfur and oxygen connections are indicated by green lines and contours.

the simulations. Only a few (13%) twisted structures appear; this behavior is typical of molecules in solution or adsorbed on adatoms. Instead, the propensity of most of the adsorbates (78%) is to maintain moderate elongations that fluctuate at approximately 21 Å. Considering that the terminal groups are protected and that the cysteine side chains are less prone to form strong intermolecular hydrogen bonds, only the atoms of the backbone are available, in principle, for interpeptide connections. These are observed just in a few cases because these atoms are also engaged in interactions with the gold layers. Interestingly, one of the adsorbed self-assembled complexes is an almost extended beta-sheet structure with persistent hydrogen bonds along the backbones that bring the peptides close together (top image in Fig. 4). Visual inspection of the final models suggests that the forces responsible for the alignment and orientation of the peptides are electrostatic and hydrophobic interactions, but the electrostatic interactions are dominant. To determine how the organization of the peptides is driven by these forces, we examined the molecular electrostatic potential (MEP) [43, 44] that is generated by the atomic partial charges on the solvent accessible surface (SAS) of the solute (Figs. S6 and S7 in the ESM). The fixed atomic partial charges derived from the ff12SB force field [38] in the AMBER12 package [45] and polarizable charges employed by the ReaxFF approach (QEq model [42]) were also compared (Fig. S8 in the ESM).

As suggested in several papers by Seminario and co-workers, the MEP is responsible for chemical recognition and represents a type of signature at the nanoscale level [46]. The color-coded MEP surfaces of the final complex shown in Fig. S6 in the ESM (the blue and red regions identify positive and negative potential, whereas the white regions identify zero values) confirm the reliable behavior of the ReaxFF–MD approach and demonstrate that the peptides polarize the metal, transfer part of their charge to the support, and form strong bonds, which is in line with quantum chemical calculations [47]. The MEPs of the peptides produced by the ReaxFF charges are very similar to those of the frozen charge model, suggesting that the parameters developed for amino acids [40] could be compared with the state-of-the-art force fields for proteins. The concerted action of all the molecular species present in the crowded environment simulated here prevent the individuation of specific components that dominate the binding process. Instead, the data analysis indicates that the adsorption is generally a sum of coexisting processes (namely charge transfer, interface dipoles, molecular deformations, and surface relaxations) that are appropriately balanced based on local conditions. All these events occur under the perturbing action of the solvent. Indeed, all the described phenomena are influenced by the surrounding water molecules. Peptide and nanoparticle solvation were examined by choosing three different layers (at 2.8, 3.4, and 5.0 Å) around all the biofunctionalized AuNPs and counting the number of water molecules within them in the final sampled snapshots (Fig. S2 in the ESM). Most of the peptides and the

nanoparticles are increasingly solvated along the production, which is in line with the partial desorption of the adsorbates and the flexibility of the structures. In contrast, the opposite effect, i.e., a gradual de-solvation of the molecules, is observed in the AuNP contact region. There, the reinforcement of peptide–peptide interactions and inter-particle association promotes the migration of water molecules toward the outer regions. The initial solvation is reduced by approximately 75%.

Moving to the results concerning the behavior of the bare AuNPs at very close distances, the induced sintering process continued after removing the constraining force, which is in line with data reported in the literature [48–51]. The nanoparticle coalescence is driven mainly by surface and grain boundary diffusions; it is very rapid and occurs within less than 100 ps. The permeation of the Au atoms of both nanoparticles starts form a limited number of contact points and then extends to larger areas. The first encounters and the slow gradual diffusion of the gold atoms in the contact regions are accompanied by progressive expulsion of the water molecules present in the gap (dehydration). The potential energy trend, shown in Fig. 5, is very similar to the ones reported by Dutta [51] and other authors [48], and can be ascribed to the elastoplastic mechanism observed in Ref. [51]. As explained by Dutta [51], surface disappearance, compression, and plastic deformations of the nanoparticles determine the initial fast energy decrease, subsequent release of stress, and stabilization.

A completely different scenario emerges for the functionalized supports. The potential energy trend and the evolution of the center of mass distances of the two AuNPs are shown in Fig. 6.

There is a trapped stress in the systems, and the interaction energy is unfavorable, even though the particles assemble appropriately by orienting their bare gold patches at short inter-particle separations. Indeed, after releasing the constraint, the AuNPs move farther apart, and their reciprocal orientation changes in such a way that the adsorbed peptides could favorably interact and remain in that arrangement until the end of the simulation. Essentially, the AuNPs regain their equilibrium configuration with optimal peptide–peptide interactions and an average minimum surface–surface separation oscillation of approximately 13 Å.

4 Conclusions

The results are relevant for confirming the observed propensity of covalent adsorption of this type of

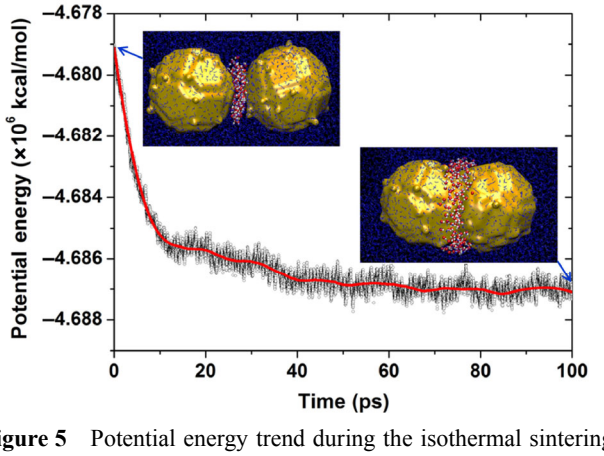

Figure 5 Potential energy trend during the isothermal sintering (unrestrained dynamics) of the AuNPs in a water solution at 300 K. The red curve is the smoothed profile. The initial configuration was obtained from the last structure sampled during the production dynamics. Peptides were removed and the centers of mass of the AuNPs were pushed at a shorter separation (around 7 Å). Initial and final configurations are shown. The water molecules in the gap between the AuNPs are visualized by means of red and white CPK models (refer to the movie in the ESM).

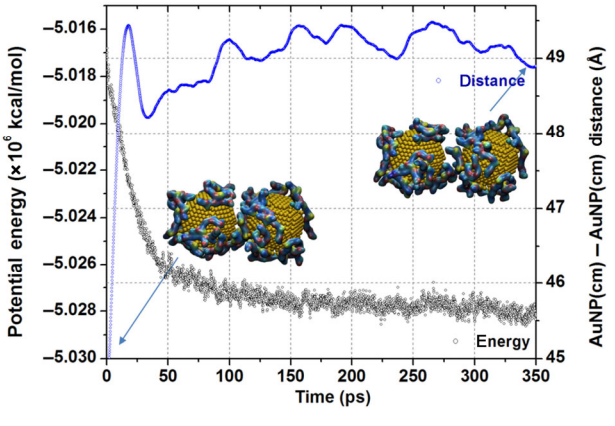

Figure 6 Potential energy trend during the isothermal sintering (unrestrained dynamics) of the functionalized AuNPs in a water solution at 300 K. The initial configuration was obtained from the last structure sampled during the production dynamics after pushing the centers of mass of the two AuNPs to shorter separations (approximately 7.4 Å). Initial and final configurations are shown. The adsorbed peptides are visualized using SASs colored according to the atom type.

peptide on the surface of AuNPs to form a layer of interconnected structures. The simulation time and abundant configurational sampling were sufficient to identify the main features of these systems, namely various adsorption modes, protonation states, intermolecular interactions, and the tendency of the complexes to form supramolecular aggregates.

All the details regarding the connections, peptide conformations, and interparticle interactions at the atomic level were disclosed. Surface decoration prevents the action of the solvent and limits surface reconstruction. Gold adatoms that migrated on top of the nanoparticle interface or to farther regions were entrapped among the peptide free chains and contributed to create a reinforced protective shell. The functionalized supports could agglomerate through electrostatic and van der Waals intermolecular interactions of the partially adsorbed molecules, but also by means of covalent cross-links of the portions of the chains that extend far from the surface because of the favorable polarity of these neutral peptides. Sintering was hindered by the action of the peptide chains that remained sparsely adsorbed, even when the interface was not completely covered.

Acknowledgements

S. M. is grateful to Adri C. T. van Duin for the stand–alone version of ReaxFF, for his support and collaboration. We acknowledge computational resources provided by the CINECA consortium (Grant ISCRA 2016 SINGOLD).

Electronic Supplementary Material: Supplementary material (details regarding the results of the MD simulations: peptide structures, radial distribution functions, radius of gyration, structures solvation, molecular electrostatic maps and atomic partial charges) is available in the online version of this article at https://doi.org/10.1007/s12274-017-1704-2.

References

[1] Monti, S.; Carravetta, V.; Ågren, H. Simulation of gold functionalization with cysteine by reactive molecular dynamics. *J. Phys. Chem. Lett.* **2016**, *7*, 272–276.

[2] Monti, S.; Carravetta, V.; Ågren, H. Decoration of gold nanoparticles with cysteine in solution: Reactive molecular dynamics simulations. *Nanoscale* **2016**, *8*, 12929–12938.

[3] Monti, S.; Carravetta, V.; Ågren, H. Theoretical study of the adsorption mechanism of cystine on Au(110) in aqueous solution. *Small* **2016**, *12*, 6134–6143.

[4] Di Felice, R.; Selloni, A. Adsorption modes of cysteine on Au(111): Thiolate, amino-thiolate, disulfide. *J. Chem. Phys.* **2004**, *120*, 4906–4914.

[5] Di Felice, R.; Selloni, A.; Molinari, E. DFT study of cysteine adsorption on Au(111). *J. Phys. Chem. B* **2003**, *107*, 1151–1156.

[6] Di Felice, R.; Corni, S. Simulation of peptide-surface recognition. *J. Phys. Chem. Lett.* **2011**, *2*, 1510–1519.

[7] Yang, X.; Yang, M. X.; Pang, B.; Vara, M.; Xia, Y. N. Gold nanomaterials at work in biomedicine. *Chem. Rev.* **2015**, *115*, 10410–10488.

[8] Falamas, A.; Tosa, N.; Tosa, V. Dynamics of laser excited colloidal gold nanoparticles functionalized with cysteine derivatives. *J. Quant. Spectrosc. Radiat. Transfer* **2015**, *162*, 207–212.

[9] Fratila, R. M.; Mitchell, S. G.; del Pino, P.; Grazu, V.; de la Fuente, J. M. Strategies for the biofunctionalization of gold and iron oxide nanoparticles. *Langmuir* **2014**, *30*, 15057–15071.

[10] Tadepalli, S.; Kuang, Z. F.; Jiang, Q. S.; Liu, K. K.; Fisher, M. A.; Morrissey, J. J.; Kharasch, E. D.; Slocik, J. M.; Naik, R. R.; Singamaneni, S. Peptide functionalized gold nanorods for the sensitive detection of a cardiac biomarker using plasmonic paper devices. *Sci. Rep.* **2015**, *5*, 16206.

[11] Raj, V.; Vijayan, A. N.; Joseph, K. Cysteine capped gold nanoparticles for naked eye detection of *E. coli* bacteria in UTI patients. *Sens. Bio-Sensing Res.* **2015**, *5*, 33–36.

[12] Miao, C. C.; Zhang, A. M.; Xu, Y. N.; Chen, S.; Ma, F. M.; Huang, C. S.; Jia, N. Q. An ultrasensitive electrochemiluminescence sensor for detecting diphenhydramine hydrochloride based on L-cysteine-functionalized multi-walled carbon nanotubes/gold nanoparticles nanocomposites. *Sens. Actuators B Chem.* **2015**, *213*, 5–11.

[13] An, D. Y.; Su, J. G.; Weber, J. K.; Gao, X. Y.; Zhou, R. H.; Li, J. Y. A peptide-coated gold nanocluster exhibits unique behavior in protein activity inhibition. *J. Am. Chem. Soc.* **2015**, *137*, 8412–8418.

[14] Sudeep, P. K.; Joseph, S. T. S.; Thomas, K. G. Selective detection of cysteine and glutathione using gold nanorods. *J. Am. Chem. Soc.* **2005**, *127*, 6516–6517.

[15] Fajín, J. L. C.; Gomes, J. R. B.; Cordeiro, M. N. D. S. DFT study of the adsorption of D-(L-)cysteine on flat and chiral stepped gold surfaces. *Langmuir* **2013**, *29*, 8856–8864.

[16] Chapman, C. R. L.; Ting, E. C. M.; Kereszti, A.; Paci, I. Self-assembly of cysteine dimers at the gold surface: A computational study of competing interactions. *J. Phys. Chem. C* **2013**, *117*, 19426–19435.

[17] Jing, C. Y.; Fang, Y. Experimental (SERS) and theoretical (DFT) studies on the adsorption behaviors of L-cysteine on gold/silver nanoparticles. *Chem. Phys.* **2007**, *332*, 27–32.

[18] Liu, W. L.; Li, C.; Tang, L.; Tong, A. Y.; Gu, Y.; Cai, R.; Zhang, L.; Zhang, Z. Q. Nanopore array derived from L-cysteine oxide/gold hybrids: Enhanced sensing platform for hydroquinone and catechol determination. *Electrochim. Acta* **2013**, *88*, 15–23.

[19] Shin, T.; Kim, K.-N.; Lee, C.-W.; Shin, S. K.; Kang, H. Self-assembled monolayer of L-cysteine on Au(111): Hydrogen exchange between zwitterionic L-cysteine and physisorbed water. *J. Phys. Chem.* B **2003**, *107*, 11674–11681.

[20] Zhao, Y. X.; Zhou, F.; Zhou, H. C.; Su, H. B. The structural and bonding evolution in cysteine-gold cluster complexes. *Phys. Chem. Chem. Phys.* **2013**, *15*, 1690–1698.

[21] Munro, C. J.; Hughes, Z. E.; Walsh, T. R.; Knecht, M. R. Peptide sequence effects control the single pot reduction, nucleation, and growth of Au nanoparticles. *J. Phys. Chem. C* **2016**, *120*, 18917–18924.

[22] Hughes, Z. E.; Walsh, T. R. Non-covalent adsorption of amino acid analogues on noble-metal nanoparticles: Influence of edges and vertices. *Phys. Chem. Chem. Phys.* **2016**, *18*, 17525–17533.

[23] Bedford, N. M.; Hughes, Z. E.; Tang, Z. H.; Li Y.; Briggs, B. D.; Ren, Y.; Swihart, M. T.; Petkov, V. G.; Naik, R. R.; Knecht, M. R. et al. Sequence-dependent structure/function relationships of catalytic peptide-enabled gold nanoparticles generated under ambient synthetic conditions. *J. Am. Chem. Soc.* **2016**, *138*, 540–548.

[24] Wright, L. B.; Palafox-Hernandez, J. P.; Rodger, P. M.; Corni, S.; Walsh, T. R. Facet selectivity in gold binding peptides: Exploiting interfacial water structure. *Chem. Sci.* **2015**, *6*, 5204–5214.

[25] Chen, G. C.; Xie, Y. S.; Peltier, R.; Lei, H. P.; Wang, P.; Chen, J.; Hu, Y.; Wang, F.; Yao, X.; Sun, H. Y. Peptide-decorated gold nanoparticles as functional nano-capping agent of mesoporous silica container for targeting drug delivery. *ACS Appl. Mater. Interfaces* **2016**, *8*, 11204–11209.

[26] Hughes, Z. E.; Nguyen, M. A.; Li, Y.; Swihart, M. T.; Walsh, T. R.; Knecht, M. R. Elucidating the influence of materials-binding peptide sequence on Au surface interactions and colloidal stability of Au nanoparticles. *Nanoscale* **2017**, *9*, 421–432.

[27] Briggs, B. D.; Palafox-Hernandez, J. P.; Li, Y.; Lim, C.-K.; Woehl, T. J.; Bedford, N. M.; Seifert, S.; Swihart, M. T.; Prasad P. N.; Walsh, T. R. et al. Toward a modular multi-material nanoparticle synthesis and assembly strategy via bionanocombinatorics: Bifunctional peptides for linking Au and Ag nanomaterials. *Phys. Chem. Chem. Phys.* **2016**, *18*, 30845–30856.

[28] Tofanello, A.; Miranda, É. G. A.; Dias, I. W. R.; Lanfredi, A. J. C.; Arantes, J. T.; Juliano, M. A.; Nantes, I. L. pH-dependent synthesis of anisotropic gold nanostructures by bioinspired cysteine-containing peptides. *ACS Omega* **2016**, *1*, 424–434.

[29] Rai, M.; Ingle, A. P.; Gupta, I.; Brandelli, A. Bioactivity of noble metal nanoparticles decorated with biopolymers and their application in drug delivery. *Int. J. Pharm.* **2015**, *496*, 159–172.

[30] Iqbal, M.; Zafar, N.; Fessi, H.; Elaissari, A. Double emulsion solvent evaporation techniques used for drug encapsulation. *Int. J. Pharm.* **2015**, *496*, 173–190.

[31] Goyal, R.; Macri, L. K.; Kaplan, H. M.; Kohn, J. Nanoparticles and nanofibers for topical drug delivery. *J. Control. Release* **2016**, *240*, 77–92.

[32] Scarì, G.; Porta, F.; Fascio, U.; Avvakumova, S.; Dal Santo, V.; De Simone, M.; Saviano, M.; Leone, M.; Del Gatto, A.; Pedone, C. et al. Gold nanoparticles capped by a GC-containing peptide functionalized with an RGD motif for integrin targeting. *Bioconjugate Chem.* **2012**, *23*, 340–349.

[33] Porta, F.; Speranza, G.; Krpetić, Ž.; Dal Santo, V.; Francescato, P.; Scarì, G. S. Gold nanoparticles capped by peptides. *Mater. Sci. Eng. B* **2007**, *140*, 187–194.

[34] Krpetić, Ž.; Nativo, P.; Porta, F.; Brust, M. A multidentate peptide for stabilization and facile bioconjugation of gold nanoparticles. *Bioconjugate Chem.* **2009**, *20*, 619–624.

[35] Aili, D.; Selegård, R.; Baltzer, L.; Enander, K.; Liedberg, B. Colorimetric protein sensing by controlled assembly of gold nanoparticles functionalized with synthetic receptors. *Small* **2009**, *5*, 2445–2452.

[36] Chen, P.; Selegård, R.; Ailic, D.; Liedberg, B. Peptide functionalized gold nanoparticles for colorimetric detection of matrilysin (MMP–7) activity. *Nanoscale* **2013**, *5*, 8973–8976.

[37] Li, X.; Carravetta, V.; Li, C.; Monti, S.; Rinkevicius, Z.; Ågren, H. Optical properties of gold nanoclusters functionalized with a small organic compound: Modeling by an integrated quantum-classical approach. *J. Chem. Theory Comput.* **2016**, *12*, 3325–3339.

[38] Zgarbová, M.; Otyepka, M.; Šponer, J.; Mládek, A.; Banáš, P.; Cheatham III, T. E.; Jurečka, P. Refinement of the Cornell et al. nucleic acids force field based on reference quantum chemical calculations of glycosidic torsion profiles. *J. Chem. Theory Comput.* **2011**, *7*, 2886–2902.

[39] Case, D. A.; Darden, T. A.; Iii, T, E, C.; Simmerling, C. L.; Wang, J.; Duke, E. H. M.; Luo, R.; Walker, R. C.; Zhang, W.; Merz, K. M. et al. *Amber 12*; University of California: San Francisco, CA, 2012.

[40] Monti, S.; Corozzi, A.; Fristrup, P.; Joshi, K. L.; Shin, Y. K.; Oelschlaeger, P.; van Duin, A. C. T.; Barone, V. Exploring the conformational and reactive dynamics of biomolecules in solution using an extended version of the glycine reactive force field. *Phys*. *Chem*. *Chem*. *Phys*. **2013**, *15*, 15062–15077.

[41] Berendsen, H. J. C.; Postma, J. P. M.; Van Gunsteren, W. F.; DiNola, A.; Haak, J. R. Molecular dynamics with coupling to an external bath. *J*. *Chem*. *Phys*. **1984**, *81*, 3684–3690.

[42] Plimpton, S. Fast parallel algorithms for short-range molecular dynamics. *J*. *Comput*. *Phys*. **1995**, *117*, 1–19.

[43] Tour, J. M.; Kozaki, M.; Seminario, J. M. Molecular scale electronics: A synthetic/computational approach to digital computing. *J*. *Am*. *Chem*. *Soc*. **1998**, *120*, 8486–8493.

[44] Miao, L.; Seminario, J. M. Molecular dynamics simulations of the vibrational signature transfer from a glycine peptide chain to nanosized gold clusters. *J*. *Phys*. *Chem*. *C* **2007**, *111*, 8366–8371.

[45] Salomon-Ferrer, R.; Case, D. A.; Walker, R. C. An overview of the amber biomolecular simulation package. *Comput*. *Mol*. *Sci*. **2013**, *3*, 198–210.

[46] Kumar, N.; Seminario, J. M. Design of nanosensors for fissile materials in nuclear waste water. *J*. *Phys*. *Chem*. *C* **2013**, *117*, 24033–24041.

[47] Höffling, B.; Ortmann, F.; Hannewald, K.; Bechstedt, F. Single cysteine adsorption on Au(110): A first-principles study. *Phys*. *Rev*. *B* **2010**, *81*, 045407.

[48] Zeng, P.; Zajac, S.; Clapp, P. C.; Rifkin, J. A. Nanoparticle sintering simulations. *Mater*. *Sci*. *Eng*. *A* **1998**, *252*, 301–306.

[49] Koparde, V. N.; Cummings, P. T. Molecular dynamics simulation of titanium dioxide nanoparticle sintering. *J*. *Phys*. *Chem*. *B* **2005**, *109*, 24280–24287.

[50] Koparde, V. N.; Cummings, P. T. Phase transformations during sintering of titania nanoparticles. *ACS Nano* **2008**, *2*, 1620–1624.

[51] Dutta, A. Kinetics of neck formation during nanoparticle sintering: Approach of dimensionality reduction. *Rev*. *Adv*. *Mater*. *Sci*. **2014**, *39*, 25–33.